Neuron, Vol. 47, 379–393, August 4, 2005, Copyright ©2005 by Elsevier Inc. DOI 10.1016/j.neuron.2005.06.027

The GTPase dMiro Is Required for Axonal Transport of Mitochondria to *Drosophila* Synapses

Xiufang Guo,[1,6,7] Greg T. Macleod,[1,5,7] Andrea Wellington,[1] Fangle Hu,[1,3] Sarvari Panchumarthi,[1,3] Miriam Schoenfield,[1,4] Leo Marin,[5] Milton P. Charlton,[5] Harold L. Atwood,[5] and Konrad E. Zinsmaier[1,2,*]

[1]Arizona Research Laboratories
Division of Neurobiology
[2]Department of Molecular and Cellular Biology
[3]Program in Molecular & Cellular Biology
[4]Undergraduate Biology Research Program
University of Arizona
Tucson, Arizona 85721
[5]Department of Physiology
University of Toronto
Toronto, Ontario M5S 1A8
Canada
[6]Program in Neuroscience
University of Pennsylvania School of Medicine
Philadelphia, Pennsylvania 19104

Summary

We have identified EMS-induced mutations in *Drosophila* Miro (dMiro), an atypical mitochondrial GTPase that is orthologous to human Miro (hMiro). Mutant *dmiro* animals exhibit defects in locomotion and die prematurely. Mitochondria in *dmiro* mutant muscles and neurons are abnormally distributed. Instead of being transported into axons and dendrites, mitochondria accumulate in parallel rows in neuronal somata. Mutant neuromuscular junctions (NMJs) lack presynaptic mitochondria, but neurotransmitter release and acute Ca^{2+} buffering is only impaired during prolonged stimulation. Neuronal, but not muscular, expression of dMiro in *dmiro* mutants restored viability, transport of mitochondria to NMJs, the structure of synaptic boutons, the organization of presynaptic microtubules, and the size of postsynaptic muscles. In addition, gain of dMiro function causes an abnormal accumulation of mitochondria in distal synaptic boutons of NMJs. Together, our findings suggest that dMiro is required for controlling anterograde transport of mitochondria and their proper distribution within nerve terminals.

Introduction

Mitochondria are critical for aerobic respiration, Ca^{2+} homeostasis, and apoptosis. The activity and subcellular distribution of mitochondria are not static, but adaptable to physiological stresses and changes in the metabolic demands of the cell (Karbowski and Youle, 2003; Rintoul et al., 2003; Hollenbeck, 1996). Control of mitochondrial distribution is believed to be especially important for neurons because of their high metabolic demands and their complex polar morphology (e.g., axons, dendrites, and synapses). Neuronal mitochondria are enriched in regions of intense energy consumption, including mobile growth cones, nodes of Ranvier, and synaptic terminals (Bindokas et al., 1998; Shepherd and Harris, 1998; Morris and Hollenbeck, 1993; Wong-Riley and Carroll, 1984; Wong-Riley and Welt, 1980). For example, synaptic terminals may consume up to 10% of the total energy required for neuronal signaling (Laughlin, 2001). Consistently, loss of mitochondria from photoreceptor terminals is associated with blindness and a failure of synaptic transmission in the *Drosophila* mutant *milton* (Stowers et al., 2002). In cultured hippocampal neurons, the number of dendritic mitochondria correlates with the number and plasticity of dendritic spines and synapses (Li et al., 2004). In addition, mitochondrial transport responds specifically to growth cone activity and nerve growth factor signaling (Chada and Hollenbeck, 2004). Together, these studies underscore the functional significance of controlling the subcellular targeting of mitochondria.

The molecular mechanisms that control the subcellular distribution of mitochondria involve long-distance transport along microtubules (MTs), which provide polar tracks for plus end-directed kinesin and minus end-directed dynein motor proteins. Mitochondria, like vesicles, display bidirectional motion where the cargo stops, starts, and often changes direction (Welte, 2004; Vale, 2003; Hollenbeck, 1996). Assuming that mitochondria are simultaneously attached to two opposing motors (De Vos et al., 2003), then net movement in one direction may be determined by the motor with the overall highest activity or, alternatively, only one of the motors may be engaged with the MT track (Welte, 2004). However, the molecular mechanisms that achieve specificity, directionality, and temporal control of mitochondrial transport in response to intracellular signals remain poorly understood. A better understanding is highly desirable, as vulnerabilities of transport systems to genetic and/or environmental insults often result in human neurological or neurodegenerative diseases (Goldstein, 2003; Crosby and Proukakis, 2002; Goldstein, 2001).

The mitochondrial Rho-GTPase (Miro) protein family may have the potential to link cellular signaling pathways with mitochondrial dynamics and function. Orthologs of human Miro (hMiro1 and 2) are all characterized by the presence of two different GTPase domains and two Ca^{2+} binding EF hand domains (Frederick et al., 2004; Fransson et al., 2003). Overexpression of constitutively active human Miro in COS7 cells causes perinuclear mitochondrial aggregates and increased apoptosis (Fransson et al., 2003). Yeast cells lacking Miro (Gem1p) reveal a collapse of the tubular mitochondrial network that is not caused by defects in mitochondrial fission and/or fusion. Genetic studies further indicate that both GTPase domains and both EF-hand motifs are required for Gem1p function (Frederick et al., 2004).

We have carried out a genetic screen for mutations

*Correspondence: kez@neurobio.arizona.edu
[7]These authors contributed equally to this work.

that affect synaptic structure and function in *Drosophila*. From this screen, we have identified lethal mutations in *Drosophila* Miro (dMiro). Our molecular and genetic analyses suggest that dMiro is required for anterograde axonal transport of mitochondria and their proper subcellular distribution. Although *dmiro* mutant motor terminals are structurally deformed and chronically lack mitochondria, they can sustain neurotransmitter release at basic levels, but fatigue during high-frequency stimulation. While presynaptic Ca^{2+} resting levels are elevated, abnormal accumulations of Ca^{2+} occur only during prolonged periods of repetitive stimulation.

Results

Identification of Mutations in the *dmiro* Gene

We have employed genetic screens to identify previously unknown genes required for axonal and synaptic function in *Drosophila*. To bypass the inefficiency of lethal F3-screening methods, we took advantage of the EGUF/Hid method (Stowers and Schwarz, 1999), which produces genetically mosaic flies in which only the eye is exclusively composed of cells homozygous for the mutation. Since "blindness" is caused by a loss of either phototransduction, nerve excitation, or synaptic function, we screened for "blind" flies by assaying the phototactic behavioral response of *Drosophila,* using the "counter-current apparatus" (Benzer, 1967). Targeting chromosome 3R, we screened ~13,000 EMS-mutagenized F1 flies and recovered 102 mutations that disrupt phototaxis, but do not grossly affect eye morphology. Genetic complementation analysis revealed a total of 53 lethal complementation groups, which were further characterized by their genetic map position and their synaptic defects at larval NMJs.

We selected the lethal mutation *B682* for further analysis because it caused an unusual activity-dependent defect in synaptic transmission and a lack of mitochondria at nerve terminals. Deletion mapping limited the *B682* locus to a region containing 17 mostly predicted genes at chromosomal position 95D7-11 (Figure 1A). An independent genetic screen had also identified four lethal EMS-induced alleles that mapped to 95D7-11 and caused defects in synaptic transmission (Babcock et al., 2003). Further genetic analysis revealed that *B682* failed to complement the lethality of all four alleles (See Table S1 in the Supplemental Data available with this article online), suggesting that all five alleles disrupt the same gene.

Identification of the mutated gene was facilitated by genetic fine mapping of the *B682* mutation using site-specific male recombination (Chen et al., 1998). The data placed the *B682* locus between two P insertion sites, containing three predicted genes (Figure 1A). Further genetic analysis excluded one flanking gene (data not shown), leaving only two viable candidates: CG5977, the fly homolog of human Spastin (Sherwood et al., 2004; Trotta et al., 2004; Kammermeier et al., 2003) and CG5410, the fly ortholog of human Miro (Fransson et al., 2003).

Sequencing of the *spastin* and *miro* genes in all five alleles, using genomic DNA and RT-PCR-derived cDNA, revealed that four of the alleles (*B682*, *sd23*, *sd26*, and *sd32*) contained mutations in *Drosophila miro* (*dmiro*), but not in the *spastin* gene (Figure 1C). One allele, *sd10*, exhibited mutations in both genes and is molecularly a double mutant. The *dmiro* and *dspastin* genes are transcribed in opposite directions, but are only separated by ~306 bp. To exclude effects of *dmiro* mutations on *spastin* expression, we examined *spastin* RNA expression by RT-PCR. Only the predicted double mutant *sd10* showed reduced *spastin* RNA expression (data not shown). Together, the molecular and genetic data consistently suggest that the alleles *B682, sd23*, *sd26*, and *sd32* are single gene mutations of the *dmiro* gene. The premature truncation of dMiro protein in *B682* and *sd32* within the first GTPase domain suggests that both alleles are presumably null mutations. Consistently, phenotypes of homozygous *B682* and *sd32* mutants were indistinguishable from those of

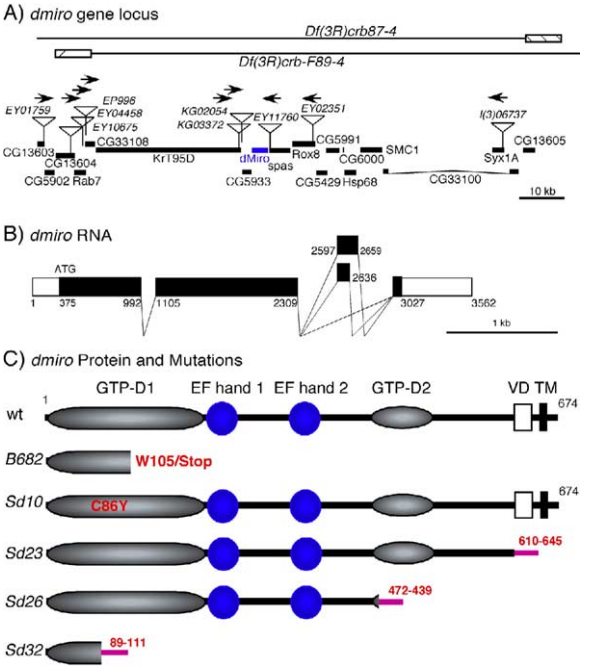

Figure 1. Genetic and Molecular Analysis of the *dmiro* Gene

(A) Map of the *dmiro* gene locus. Breakpoints of the deficiencies uncovering the *dmiro* locus are indicated. Triangles indicate P elements. Arrows show the relative map position of the *dmiro* locus, as it was obtained by male recombination mapping for each P element. Closed rectangles indicate the position of genes.

(B) Exon/intron structure of the *dmiro* gene. RT-PCR revealed expression of three differently spliced mRNA transcripts.

(C) Position of EMS-induced point mutations in dMiro. The two GTPase domains (GTP-D1 and GTP-D2) and two EF-hands (1 and 2) are indicated. VD indicates a variable domain due to alternative RNA splicing (see [B]). TM indicates a transmembrane domain. The mutation *B682* changes W105 to a UAG stop codon. *Sd23* causes a G/A substitution, generating an abnormal RNA splice site, as confirmed by RT-PCR, which frameshifts the protein after 610 amino acids (aa) and adds 35 abnormal aa (shown in red). *Sd26* causes a 39 bp deletion and frameshifts dMiro at I427, adding 12 abnormal aa. *Sd32* causes a 29 bp deletion and frameshifts dMiro at Y89, adding 12 abnormal aa before terminating. *Sd10* causes a C86Y substitution and a deletion of 61 bp in the 3′ UTR of the fly *spastin* gene (data not shown).

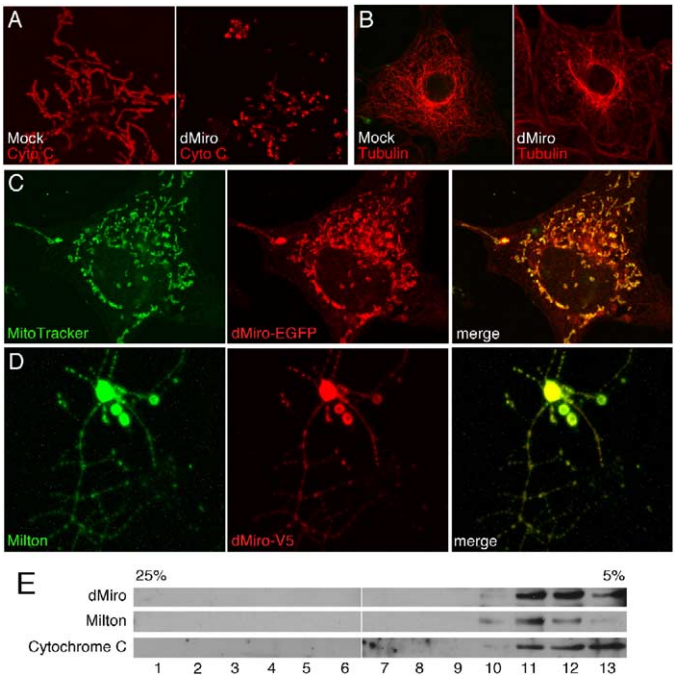

Figure 2. Ectopically Expressed dMiro Protein Colocalizes with Mitochondria

(A) Strong overexpression of dMiro-EGFP in COS7 cells disrupted the mitochondrial distribution and caused a loss of mitochondria. COS7 cells were transiently transfected with dMiro-EGFP and imaged 2 to 3 days later. Mitochondria (red) were visualized with anti-cytochrome c antibodies.

(B) Strong overexpression of dMiro-EGFP in COS7 cells had no detectable effect on MTs (red) as visualized by anti-tubulin antibodies.

(C) In weakly transfected COS7 cells the mitochondrial distribution was maintained, and dMiro-EGFP (red) colocalized with mitochondria (green).

(D) dMiro-V5 (red) colocalized with the mitochondrial marker Milton (green) in cultured *Drosophila* neurons from larval ventral ganglia expressing dMiro-V5 with a neuron-specific APP-Gal4 driver. dMiro-V5 and Milton were visualized with antibody stainings.

(E) The distributions of dMiro and the mitochondrial markers cytochrome c and Milton are indistinguishable in 5%–25% glycerol gradient fractions from adult fly head extracts.

transheterozygous combinations involving the deletion *Df(3R)mbc-R*.

The Atypical GTPase dMiro Is Associated with Mitochondria

The *dmiro* gene spans ~3.5 kb of genomic DNA, consists of four exons, and expresses at least three mRNA transcripts derived by alternative splicing of exon 3 (Figure 1B). The predicted dMiro protein sequences are orthologous (51% identity; 330/645) to human Miro (Fransson et al., 2003). Miro proteins contain two different GTPase domains and two conserved EF-hand domains (Figure 1C). The N-terminal GTPase domain of dMiro is most closely related to Rho-GTPases, while the second GTPase domain is related more to Rab-GTPases (data not shown). Like the human and yeast orthologs, dMiro contains a conserved transmembrane (TM) domain at its C terminus, which in yeast tail-anchors Miro in the outer mitochondrial membrane such that the functional domains are exposed to the cytoplasm (Frederick et al., 2004).

To verify the predicted mitochondrial localization for dMiro, we examined the subcellular localization of EGFP-tagged dMiro protein in transiently transfected COS7 cells. Strong ectopic overexpression of dMiro-EGFP disrupted the subcellular mitochondrial distribution and caused a loss of mitochondria, but did not grossly affect MTs (Figures 2A and 2B). Many cells also showed signs of apoptotic cell death (data not shown). To minimize these dominant effects on protein localization, for analysis we used only weakly transfected COS7 cells in which ectopically expressed dMiro colocalized with mitochondria that exhibited a relatively normal distribution (Figure 2C). To confirm a mitochondrial localization in *Drosophila*, we generated neuronal cell cultures from larval brains transgenically expressing V5-tagged dMiro protein. Double immunolabeling showed that tagged dMiro protein colocalized with the mitochondrial protein Milton (Stowers et al., 2002) in neuronal cell bodies and in small punctae in neurites (Figure 2D), which are reminiscent of mitochondria. Subcellular fractionation of *Drosophila* head extracts, using glycerol gradients, showed that dMiro, Milton, and cytochrome c copurify in mitochondrial fractions (Figure 2E). Together, these studies confirm that dMiro is associated with mitochondria.

Loss of dMiro Progressively Impairs Larval Locomotion

dmiro is an essential gene, since all examined *dmiro* alleles are recessive larval to early-pupal lethals (Table S1). Homozygous *dmiro* mutant larvae are slim and exhibit abnormal locomotion (Figures S1A and S1B). Control larvae crawl steadily in a given direction, showing rhythmic muscle contractions that run over the entire body. In contrast, homozygous *dmiro* larvae tend to wiggle on the spot and gain little distance (Figure S1B). Posterior segments of *dmiro* larvae appear to be excessively sluggish and sometimes even paralyzed, while anterior segments are often excessively bent, as if to compensate for failing muscle contractions in the more posterior segments. This abnormal crawling behavior indicates a progressive weakness of the larval body-wall musculature that originates at posterior segments and eventually leads to paralysis.

Loss of dMiro Disrupts the Subcellular Distribution of Mitochondria in Neurons and Muscles

To test whether *dmiro* mutations affect mitochondria, we imaged live mitochondria by visualizing mitochondria selectively in neurons or muscles, using a modified GFP that specifically labels mitochondria (Mi-

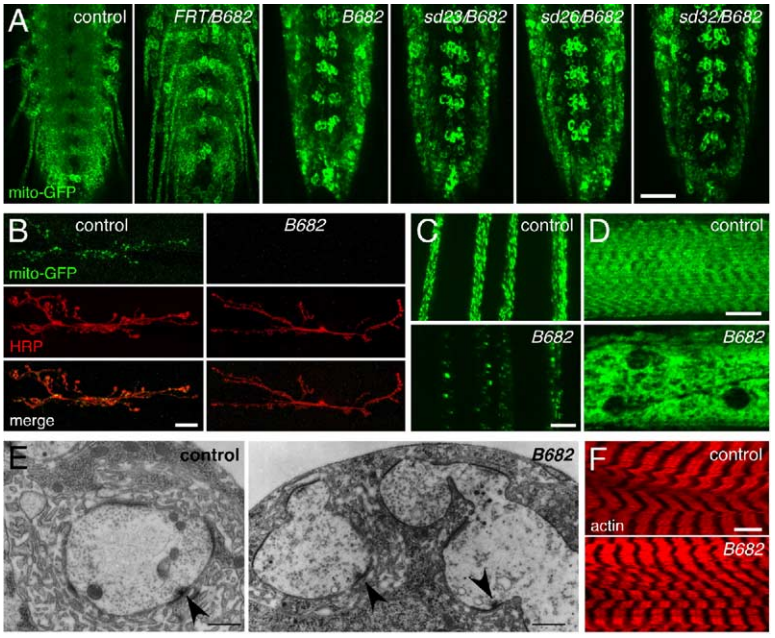

Figure 3. Abnormal Distribution of GFP-Tagged Mitochondria in *dmiro* Mutant Neurons and Muscles

(A) Distribution of neuronal mitochondria in ventral ganglia from third instar larvae. Mitochondria accumulate in neuronal cell bodies and are lost in segmental nerves of *dmiro* mutants. Neuronal mitochondria were visualized by expression of MitoGFP (green) with the neuronal Gal4 driver *elav*. Genotypes are indicated. Scale bar, 50 μm.

(B) Presynaptic mitochondria (MitoGFP, green) are absent at *dmiro* mutant NMJs. NMJs were counterstained with anti-HRP antibodies (red) to visualize neuronal membranes. Scale bar, 20 μm.

(C) Mitochondria are reduced in segmental nerves in proximity to *dmiro* mutant ventral ganglia. Scale bar, 20 μm.

(D) Abnormal distribution of mitochondria (green) in muscle 6 of *dmiro* mutant larvae. MitoGFP was expressed by the 24B-Gal4 driver. Scale bar, 20 μm.

(E) Representative electron microscopic images of type 1b boutons from control and *dmiro* mutant larval NMJs 6/7. Note the absence of mitochondria, the often diffuse distribution of synaptic vesicles, and the abnormal subdivision of *dmiro* mutant boutons. Arrowheads indicate synapses containing "T-bars." Scale bar, 500 nm.

(F) Actin-phalloidin staining of control and *dmiro* mutant larval muscles showed no differences, indicating normal arrangement of sarcomeres. Scale bar, 10 μm.

toGFP). Neuronal expression of MitoGFP revealed an abnormal distribution of neuronal mitochondria in ventral ganglia of *dmiro* mutant larvae. In contrast to controls, MitoGFP fluorescence in *dmiro* mutants was enriched in neuronal somata, but reduced in the neuropil (Figure 3A), reduced in segmental nerves close to the ganglia (Figure 3C), and absent in more distal nerve regions. At larval NMJs, presynaptic MitoGFP fluorescence was, in general, not detectable (Figure 3B); only rarely mutant NMJs showed one or two punctae of GFP fluorescence while almost all synaptic boutons of control NMJs were labeled (Figure 3B). The absence of presynaptic mitochondria at larval NMJs of *dmiro* mutants was confirmed by live dye staining using MitoTracker dyes (data not shown) and by an ultrastructural analysis (Figures 3E and 5D). Together, these results demonstrate that *dmiro* mutant mitochondria are retained in neuronal cell bodies and are not properly distributed into neuronal processes.

Muscle-specific expression of MitoGFP revealed a highly regular and stereotypical pattern of mitochondria in control muscles (Figure 3D), which is reminiscent of the pattern revealed by actin-phalloidin stainings (Figure 3F). While the distribution of actin was normal in *dmiro* mutant muscles, the mitochondrial distribution was severely disrupted: mitochondria were found in small clusters that were distributed over the entire muscle (Figure 3D). The abnormal mitochondrial clusters in mutant muscles were not associated with nuclei, which contrasts with the abnormal, perinuclear mitochondrial clusters in mutant neurons.

A Traffic Jam Arrests Axonal Transport of Mitochondria in Neuronal Somata of *dmiro* Mutants

An ultrastructural analysis provided further insights into the nature of the mitochondrial accumulations in neuronal somata. Sections of proximal larval nerves showed reduced numbers of mitochondria in axons and in the processes of glial cells of *dmiro* mutants in comparison to control larvae (Figures 4A and 4B). Reduced numbers of mitochondria were also found in the neuropil of *dmiro* mutant ventral ganglia (Figures 4C and 4D). In contrast, neuronal somata of *dmiro* mutants exhibited increased numbers of mitochondria, while control neuronal somata contained few mitochondria. Specifically, *dmiro* mutant somata showed large, organized clusters of mitochondria, which were variable in size and close to Golgi apparati (Figures 4E–4I). Within these clusters, mitochondria were neatly lined up in parallel rows, like "strings of pearls." In many cases, the mitochondria within a string showed a similar orientation of their cristae (Figure 4H). The occurrence of organized mitochondrial clusters in *dmiro* mutants has two implications: first, the "string of pearls" appearance suggests that the clustered mitochondria are associated with the cytoskeleton, presumably with MTs; and second, it suggests that a MT-associated "roadblock" or impaired anterograde motor activity may arrest anterograde mitochondrial transport.

Structural and/or functional changes in mitochondria often cause a redistribution of mitochondria and could also account for the defect in mitochondrial transport of *dmiro* mutants (Miller and Sheetz, 2004; Chen et al., 2003; Karbowski and Youle, 2003). However, our EM analysis revealed no noticeable ultrastructural defects of mitochondria in *dmiro* mutants (Figures 4H and 4I). In addition, mitochondria in cultured neurons from both *dmiro* mutant and control ganglia showed similar intensities of MitoTracker staining (Figures S2A and S2B). Finally, labeling of mitochondria with JC-1 dye showed no abnormalities in the membrane potential of *dmiro*

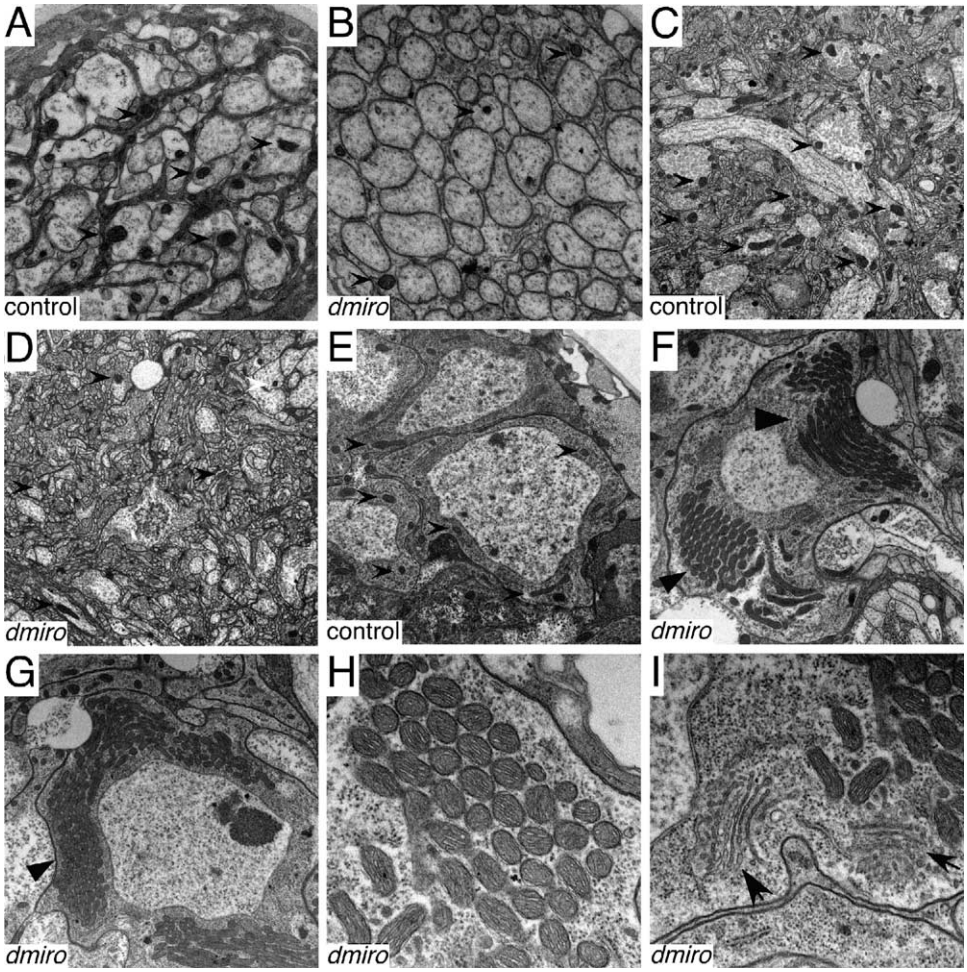

Figure 4. Mitochondria Form Organized Clusters in Neuronal Somata of *dmiro* Mutants

(A and B) Ultrastructure of proximal third instar segmental nerves in control (A) and $dmiro^{B682}$ mutants (B). Note the reduced number of mitochondria (arrowheads) in *dmiro* mutant axons and glial processes.

(C and D) Mitochondria in the neuropil of control (C) and $dmiro^{B682}$ third instar ventral ganglia (D). Note the reduction in number of mitochondria in the *dmiro* neuropil.

(E–G) Mitochondria in neuronal cell somata of control (E) and $dmiro^{B682}$ (F and G). Note the increased number and highly ordered clustering of mitochondria (closed triangles) in *dmiro* mutant cell bodies.

(H) Higher magnification of mitochondrial clusters in *dmiro* mutant cell bodies. Note the similar orientation of mitochondrial cisternae.

(I) Golgi apparati (arrows) are found close to mitochondrial clusters in *dmiro* mutant cell bodies.

mutant mitochondria (Figure S2C). Hence, it is unlikely that structural or functional changes of mitochondria underlie the abnormal transport of mitochondria in *dmiro* mutants.

Vesicular Transport Is Impaired, but Not Blocked, in *dmiro* Mutants

To test whether the arrest of mitochondrial transport in *dmiro* mutants correlates with a defect in vesicular transport, we examined larval nerves for the presence of abnormal accumulations of synaptic vesicles, as they are typically associated with mutations affecting axonal transport (Gunawardena and Goldstein, 2001; Bowman et al., 2000; Hurd and Saxton, 1996). Immunostainings of *dmiro* mutant larval nerves revealed a significant accumulation of immunopositive punctae for the synaptic vesicle protein cysteine string protein (CSP; $p < 0.01$; Figures S3A and S3C) and synaptotagmin (data not shown). However, quantification of synaptic vesicle staining at NMJs revealed no significant differences from controls (not shown), suggesting that the defect in vesicular transport is weak and does not limit vesicle supply. Similarly, immunostainings with mAb nc82, a presynaptic marker for synapses (Wucherpfennig et al., 2003), also showed an accumulation of discrete nc82-positive punctae in *dmiro* mutant nerves (Figure S3B), while the number of synapses at NMJs was not reduced (Figures 5C and 5D). Since nc82-positive punctae are very small and sparsely distributed in control nerves, the numerous large punctae in mutant nerves suggest an abnormal accumulation of transported cargo vesicles. While these data suggest that vesicular axonal transport is impaired in *dmiro* mutants, these impairments are also qualitatively and quantita-

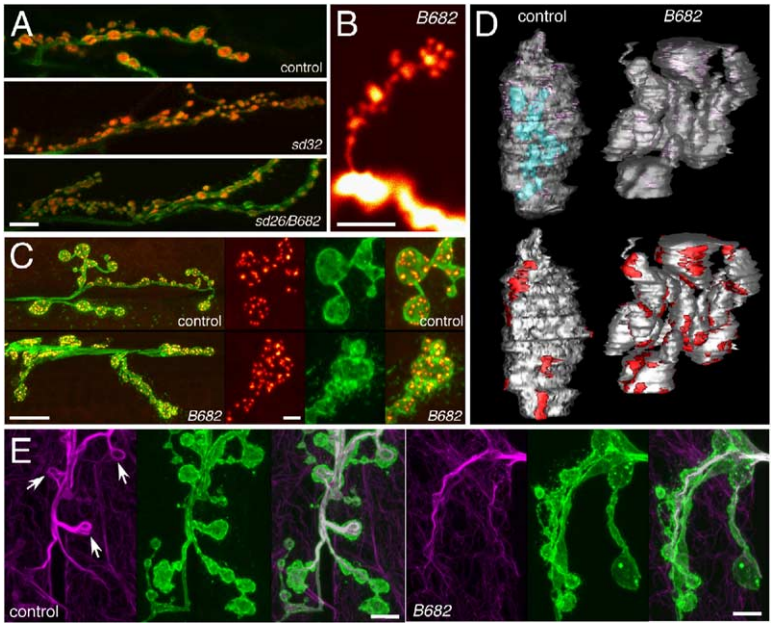

Figure 5. Abnormal Organization of Synaptic Boutons and MTs at *dmiro* Mutant NMJs

(A) Confocal images of third instar larval NMJs of muscle 6/7 that were double immunolabeled for neuronal membranes (anti-HRP, green) and synaptic vesicles (anti-CSP, red). Note a smaller bouton size and abnormal clustering of synaptic boutons in *dmiro* mutants. Genotypes are indicated. Scale bar, 10 μm.

(B) Dextran-conjugated dye filling of $dmiro^{B682}$ mutant axon terminals resolves distinct subcompartments that often surround a central compartment, giving the structure a "cauliflower-like" appearance.

(C) Double staining of control and $dmiro^{B682}$ mutant NMJs with anti-HRP (green) and mAb nc82 (presynaptic marker for synapse, orange). Note the often dense clustering of mutant synaptic boutons containing numerous synapses. Scale bars, 10 μm and 2 μm

(D) EM 3-D reconstruction using serial ultrathin sections of type 1b boutons of muscle 6/7 from control (left) and $dmiro^{B682}$ mutants (right). The images show a "transparent" view (upper) illustrating bouton shape, the localization of mitochondria (blue) and cisternae (purple), and an "opaque" view (lower) illustrating the localization of synapses (red). Note the altered bouton structure and absence of mitochondria in *dmiro*.

(E) Prominent MT loops are present in control (arrows) but not in *dmiro* mutant synaptic boutons. NMJs were double-stained with anti-HRP (green) and anti-acetylated tubulin (magenta) antibodies. Scale bar, 5 μm.

tively different from the defects in mitochondrial transport. Hence, it seems unlikely that both transport defects are caused by the impairment of a common mechanism.

Mutations in *dmiro* Alter the Structure of Synaptic Boutons and the Organization of Presynaptic MTs

Consistent with the smaller body size of *dmiro* mutant larvae, the length of larval body-wall muscles was reduced in homozygous *dmiro* mutants ($p < 0.001$). However, the normalized length of the NMJ innervating the smaller muscle (NMJ/muscle ratio) of *dmiro* mutants was generally increased to ~121% of that in controls ($p < 0.007$). In addition, *dmiro* mutant NMJs exhibited a general increase in the number of boutons to ~148% of that in controls after normalizing to the NMJ length ($p = 0.001$; Figure 5A), indicating synaptic overgrowth.

Close examination of *dmiro* mutant synaptic boutons revealed an abnormal structure. The average volume of synaptic boutons was reduced, and the distance between individual boutons was shortened such that they were often aggregated in cauliflower-like clusters. Dextran-conjugated dye fillings or double immunostainings revealed individual compartments within these clusters, containing synaptic vesicles and synapses (Figures 5A–5C). An ultrastructural 3-D reconstruction from serial sections of synaptic boutons confirmed the smaller size of *dmiro* boutons, their tendency to form densely packed clusters, and the absence of mitochondria (Figure 5D). As already indicated by immunostainings, each compartment or bouton within a cluster contained its own set of synapses (Figure 5D) and synaptic vesicles (data not shown).

To determine whether the altered bouton structure correlates with an abnormal MT cytoskeleton, we examined presynaptic MTs, using anti-HRP and anti-acetylated tubulin double stainings. Control NMJs showed robust presynaptic MT bundles extending through the entire NMJ, and large synaptic boutons exhibited easily identifiable MT loops (Figure 5E). In *dmiro* mutants the number of MT loops was significantly reduced at all examined NMJs ($p < 0.05$; Figure S4B). In contrast to controls, presynaptic MT bundles at *dmiro* mutant NMJs also often failed to extend into the last synaptic bouton of axonal branches (Figure S4A). Hence, the altered presynaptic MT cytoskeleton of *dmiro* mutant NMJs may contribute to the abnormal synaptic bouton structure.

The abnormal MT organization could be caused by the loss of dMiro activity, the loss of other mitochondrial proteins, or by a depletion of ATP due to the loss of presynaptic mitochondria. To address this, we examined MTs in *dmiro* mutant muscles where a steep ATP gradient seems unlikely because mitochondrial clusters are uniformly distributed throughout the entire muscle (Figure 3D). MTs surrounding cell nuclei appeared more pronounced in *dmiro* mutant muscles than in those of controls (Figure S4C). However, quantification of MTs surrounding individual nuclei showed no differences (data not shown), while quantification of peripheral MTs (arbitrarily defined as MTs midway between neighboring nuclei) showed a significant reduction of MT filament density in *dmiro* mutants ($p < 0.001$; Figure S4D), suggesting that MT organization in the muscle is altered under conditions in which ATP depletion is unlikely. In contrast, phalloidin staining of actin in muscles was normal in *dmiro* mutants (Figure 3F), indicating that *dmiro* mutations selectively affect the MT, but not the actin cytoskeleton.

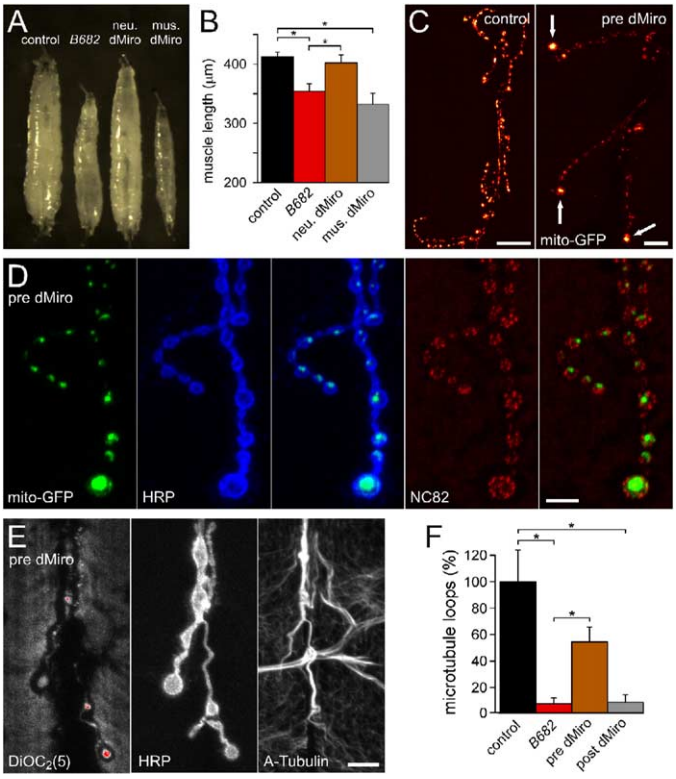

Figure 6. Neuronal Expression of Normal dMiro Reverses Defects of *dmiro* Mutant NMJs and Muscles

(A) Neuron-specific (neu-dMiro) but not muscle-specific (mus-dMiro) expression of normal dMiro protein in *dmiro*^{B682} mutants restored a normal larval body size. *UAS-dMiro* transgenes containing a cDNA for the longest RNA splice form were driven with the neuronal elav- or the muscular 24B-Gal4 driver.

(B) Neuron-specific (neu-dMiro) but not muscle-specific (mus-dMiro) expression of dMiro in *dmiro* mutants restored normal length for muscle 6. Significant differences are indicated ($p < 0.05$, $n \geq 10$, n (larvae) ≥ 5). Error bars indicate SEM.

(C) Presynaptic expression of dMiro protein (pre dMiro) in *dmiro* mutants restored mitochondrial transport to larval nerve terminals. Images show MitoGFP fluorescence from larval NMJs 6/7 of control and *dmiro*^{B682} mutant larvae expressing dMiro with the elav-Gal4 driver. Note the abnormal accumulation of mitochondria in terminal boutons of "rescued" *dmiro* mutant NMJs. Scale bar, 20 μm.

(D) Images showing higher magnification of "rescued" *dmiro* NMJs (as in [C]) that were triple-labeled to visualize mitochondria (MitoGFP, green), neuronal membranes (anti-HRP, blue), and synapses (mAb NC82, red). Note that a disproportionate accumulation, as seen for mitochondria, is not observed for synapses. Scale bar, 10 μm.

(E) Images of a "rescued" *dmiro* mutant NMJ (as in [C]) that was live-stained for mitochondria [$DiOC_2(5)$] and double-labeled after fixation with anti-HRP and anti-acetylated tubulin antibodies. Scale bar, 10 μm.

(F) Pre- but not postsynaptic expression of dMiro protein at *dmiro* mutant NMJs of muscle 6/7 reversed the lack of presynaptic MT loops. Significant differences between genotypes are indicated ($p < 0.05$, $n \geq 30$, n (larvae) ≥ 5). Error bars indicate SEM.

dMiro Is Required Presynaptically, but Not Postsynaptically, at Larval NMJs

It seemed likely that mitochondrial transport requires dMiro cell-autonomously. However, the structural defects of *dmiro* nerve terminals may have been caused by the loss of pre- or postsynaptic dMiro. To resolve this, we selectively expressed normal dMiro protein in either neurons or muscles of *dmiro* mutants, using two independent transgenes, which produced similar results. Remarkably, neuronal, but not muscular, expression of dMiro rescued the lethality of *dmiro* mutants, suggesting that dMiro activity is essential only for neuronal, but not for non-neuronal, function. In addition, neuronal, but not muscular, expression of dMiro restored normal larval body shape and muscle size (Figures 6A and 6B). Neuronal expression did not rescue the abnormal mitochondrial distribution and/or MT organization in *dmiro* mutant muscles (data not shown). Hence, the smaller body and muscle size of *dmiro* mutant larvae is not caused by muscle abnormalities, but by an abnormally functioning nervous system compromising the function of NMJs or neurosecretory terminals.

Neuronal expression of dMiro in *dmiro* mutants restored vesicular (Figure S3B) and mitochondrial transport in neurons such that mitochondria were again present at synaptic terminals of NMJs (Figures 6C–6E) and in the neuropil of ventral ganglia (data not shown). Presynaptic expression also restored normal synaptic bouton structure and reversed the absence of presynaptic MT loops at NMJs (Figures 6D–6F). However, postsynaptic expression of dMiro in *dmiro* mutant muscles neither reversed the defects in mitochondrial transport of the presynaptic neuron (data not shown) nor affected the abnormal structure of synaptic boutons (data not shown) and presynaptic MTs (Figure 6F). Together, these data suggest that dMiro is required presynaptically to supply synaptic terminals with mitochondria and ensure normal structure of the NMJ.

While presynaptic expression of dMiro restored mitochondrial transport to *dmiro* mutant nerve terminals, it did not lead to a normal distribution of mitochondria (Figures 6C–6E); mitochondria accumulated abnormally in the most distal synaptic bouton of each terminal branch and were present in reduced numbers in most of the remaining boutons. The abnormal accumulation was also observed for $DiOC_2(5)$-labeled mitochondria (Figure 6E), confirming structural mitochondrial integrity. Overexpression of dMiro in control neurons showed a similar, excessive accumulation of mitochondria in the terminal bouton of axonal branches (data not shown), suggesting that this new phenotype is caused by a gain of dMiro activity. This gain-of-function phenotype was not observed for synaptic and cargo vesicles since neither synaptic vesicles (data not shown) nor synapses were abnormally distributed (Figure 6D). Hence, reducing or increasing dMiro activity alters the subcellular distribution of mitochondria such that abnormal mito-

chondrial accumulations are switched from the cell body to the end of the axon, respectively. Accordingly, we conclude that dMiro specifically controls the activity of anterograde mitochondrial transport.

Activity-Dependent Fatigue of Synchronous Release at *dmiro* Mutant NMJs

All *dmiro* mutant alleles were identified by the loss of phototaxis of EGUF-induced mosaic flies, which was apparently caused by a defect in synaptic transmission, as indicated by the activity-dependent loss of Off transients in electroretinogram recordings from *dmiro* mutant eyes (Babcock et al., 2003). To examine in more detail the effects of the chronic loss of mitochondria on synaptic physiology, we recorded evoked excitatory junctional potentials (EJPs) and miniature excitatory junctional potentials (mEJPs) from larval NMJs. Less than half of all *dmiro* mutant muscles examined showed decreased resting potentials (< –40 mV) and/or a high rate of spontaneous quantal release. The remaining muscles exhibited a normal resting potential, deviating by no more than ± 5 mV from control, and a normal frequency of spontaneous release. Since the resting potential was normal for the majority of *dmiro* muscles, we excluded partially depolarized muscles from the subsequent analysis, because their defects were likely secondary and degenerative.

Evoked EJP amplitudes of *dmiro* mutants were normal at a low stimulation frequency of 0.2 Hz (Figure 7B). Even during prolonged stimulation at 1 Hz for 5 min, EJP amplitudes were normal (Figure 7C). However, during stimulation at 5 Hz, EJP amplitudes showed a steadily progressing fatigue after 90 s, and by 300 s, no more EJPs were elicited (Figure 7C). Consistently, higher stimulation frequencies caused a progressively earlier onset of fatigue; at 10 Hz, EJPs became depressed within 10 s, and after 15–20 s, almost all stimuli failed to elicit EJPs (Figures 7A and 7D). The activity-dependent fatigue of evoked release in *dmiro* was not due to a failure of action potentials because electrotonically elicited EJPs showed a similar fatigue (Figure 7E). A similar activity-dependent fatigue of evoked release was observed for transheterozygous combinations of *B682* with other *dmiro* alleles and a deletion uncovering the locus (Figure 7D). Presynaptic expression of dMiro at *dmiro*-null mutant NMJs restored the activity-dependent fatigue of evoked release (Figure 7D).

An activity-dependent failure of EJP amplitudes often indicates a depletion of releasable synaptic vesicles due to a defect in vesicle trafficking and/or endocytosis. However, the frequency of mEJPs at *dmiro* mutant NMJs increased up to 5-fold during high-frequency stimulation (see traces, Figure 7A) and persisted for extended periods after stimulation ($p < 0.001$; Figures 7F and 7G). The abnormal increase in mEJP frequency was activity dependent. Prolonged stimulation at 1 Hz over 5 min did not cause an increase in the frequency of unitary quantal events at *dmiro* mutant NMJs, while stimulation $\geq$5 Hz increased mEJP frequency (data not shown). Hence, the activity-dependent increase in mEJP frequencies makes it unlikely that a defect in vesicle recycling causes the fatigue of evoked release. Interestingly, similar activity-dependent effects on transmitter release were observed upon acute pharmacological inhibition of mitochondrial function and were correlated with a severe loss of presynaptic Ca^{2+} clearance (David and Barrett, 2003; Talbot et al., 2003; Nguyen et al., 1997).

Presynaptic Ca^{2+} Homeostasis at *dmiro* Mutant Motor Nerve Terminals

To test whether the activity-dependent defects in transmitter release of *dmiro* mutants are linked to an impaired presynaptic Ca^{2+} homeostasis, we examined presynaptic Ca^{2+} concentrations ($[Ca^{2+}]_i$) at *dmiro* NMJs. The resting $[Ca^{2+}]_i$ was significantly elevated from 39 ± 4.8 nM in control to 84.7 ± 11.8 nM in *dmiro* mutant terminals ($p < 0.05$; Figures 8B and 8C). However, during stimulation at 80 Hz for 5 s, the peak cytosolic $[Ca^{2+}]_i$ and the time course of $[Ca^{2+}]_i$ decay in mutant terminals were indistinguishable from those in controls. This suggests that the chronic lack of mitochondria does not affect nerve-evoked Ca^{2+} levels during brief periods of stimulation. Nerve-evoked Ca^{2+} levels during longer periods of stimulation (10 Hz/30 s) were initially similar between control and *dmiro* but progressively increased during stimulation to a significantly larger degree in *dmiro* mutants ($p < 0.05$, Figures 8D–8F), suggesting that Ca^{2+} buffering during extended periods of high activity is impaired.

Assuming that mitochondria in control terminals accumulate a significant amount of Ca^{2+} in response to nerve stimulation and subsequently slowly release it into the cytosol, one might expect that post-tetanic Ca^{2+} decay might be altered in the mutants, but this was not the case. In both mutants and controls, 3 s after stimulation ended, Ca^{2+} levels had fallen to ~8% of the plateau level achieved at the end of the stimulation train (Figures 8E and 8F), indicating that cytosolic Ca^{2+} clearance was effectively no different between strains. Hence, these results suggest that cytosolic Ca^{2+} handling is impaired only during prolonged repetitive stimulation in *dmiro* mutants, while fast Ca^{2+} clearance after stimulation is not affected. Hence, it is unlikely for two reasons that an abnormal accumulation of Ca^{2+} during 10 Hz stimulation causes the desynchronization of transmitter release in *dmiro* mutant terminals: first, stimulated Ca^{2+} levels only reached ~140 nM after 30 s of 10 Hz stimulation (Figure S5), which is in the physiological range for these terminals (Macleod et al., 2004); and second, Ca^{2+} resting levels in *dmiro* mutant terminals before and after stimulation were indistinguishable.

Activity-Dependent Ca^{2+} Uptake of Presynaptic Mitochondria at Larval Motor Nerve Terminals

Our analysis of presynaptic Ca^{2+} dynamics in nerve terminals that chronically lack mitochondria suggests only a minor role for mitochondria as presynaptic Ca^{2+} sinks, which is much in contrast to the suggested dominant role of mitochondrial Ca^{2+} sinks at other NMJs (David and Barrett, 2003, 2000; Ohnuma et al., 1999; David et al., 1998; Tang and Zucker, 1997). However, our results could be misleading for two reasons: first,

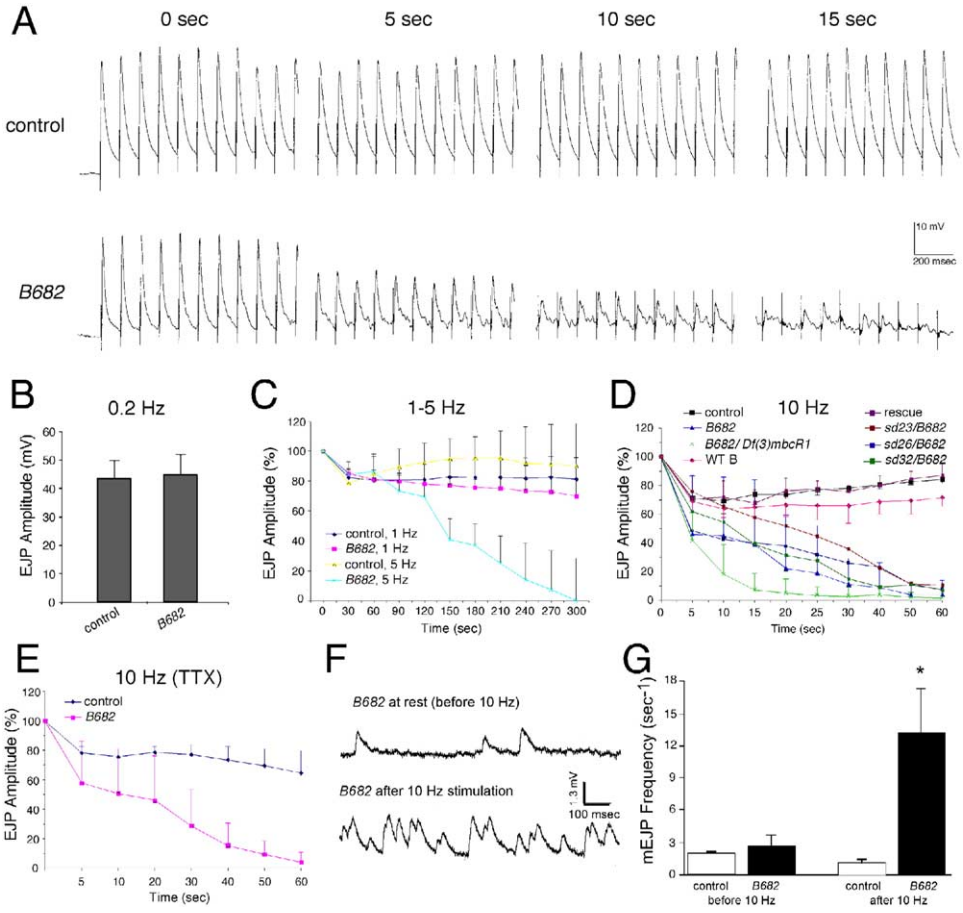

Figure 7. Activity-Dependent Fatigue of Neurotransmitter Release at *dmiro* Mutant NMJs

(A) Typical traces of EJPs that were elicited at 10 Hz and recorded from control and *dmiro*^{B682} mutant NMJs 6/7 in the presence of 1 mM Ca^{2+}. Time after onset of stimulation is indicated. (B) Mean amplitudes are shown for EJPs elicited by 0.2 Hz stimulation at control and *dmiro*^{B682} mutant NMJs. Recordings were from muscle 6 with 1 mM Ca^{2+}. (C) Normalized EJP amplitudes elicited by 1 Hz and 5 Hz stimulation for 5 min for control and *dmiro*^{B682}. No significant differences were observed for 1 Hz stimulation. Note the significant fatigue of EJP amplitudes in *dmiro* mutants after ~120 s of 5 Hz stimulation. Genotypes are indicated. (D) Normalized amplitudes of EJPs elicited at 10 Hz. Significant differences were observed after 10 s of stimulation ($p < 0.05$, $n \geq 3$). For rescue, expression of normal dMiro was driven by an elav-Gal4 driver in homozygous *dmiro*^{B682} larvae. Genotypes are indicated. Error bars were omitted for *sd23*, *sd26* and *sd32*, to allow clarity of the graph. (E) Normalized amplitudes of electrotonically elicited EJPs (10 Hz) in the presence of TTX and 1 mM Ca^{2+}. No significant difference in EJP fatigue between electrotonically and nerve-evoked (in [D]) *dmiro*^{B682} EJPs was noted. (F) Activity-dependent increase in the frequency of unitary quantal release during repetitive stimulation in *dmiro* mutants. Typical trace shows mEJPs recorded from homozygous *dmiro*^{B682} NMJs before and after 10 Hz stimulation. (G) Mean mEJP frequencies for control and *dmiro*^{B682} before and after 10 Hz stimulation. Recordings were from muscle 6 with 1 mM Ca^{2+}. Significant differences are indicated ($p < 0.05$, $n = 6$). Error bars represent SD.

mitochondria at larval *Drosophila* motor terminals may not sequester Ca^{2+} during stimulation; second, other mechanisms may compensate for the chronic lack of mitochondrial Ca^{2+} sinks. To test the first possibility, we examined mitochondrial Ca^{2+} uptake at presynaptic terminals of wild-type NMJs by employing the Ca^{2+} indicator dihydrorhod-2 AM (rhod-2), which accumulates specifically in mitochondria (Trollinger et al., 1997).

At rest, rhod-2 produced little measurable fluorescence, presumably due to low Ca^{2+} levels in mitochondria since rhod-2 fluorescence below 100 nM Ca^{2+} is effectively invisible in vitro (Molecular Probes). Upon high-frequency nerve stimulation (80 Hz, 2 s), bright fluorescent punctae appeared that were within synaptic boutons and had the same size and distribution as live-stained mitochondria (Figures 9A–9C). The activity-dependent increase in the intensity of rhod-2 fluorescence was dependent on the onset, but not on the offset, of nerve stimulation; rhod-2 fluorescence faded slowly after stimulation had ceased and became invisible only after ~5 to 10 min (Figures 9D–9F). The slow decay of rhod-2 fluorescence is consistent with a slow release of mitochondrial Ca^{2+} and contrasts with the exceedingly rapid time course of decay of cytosolic Ca^{2+} indicators, like rhodamine-dextran or transgenically expressed G-CaMP (Figure 9F). Hence, we conclude that presynaptic mitochondria at *Drosophila* NMJs can sequester Ca^{2+} in response to high-frequency nerve stimulation. However, as suggested by the relatively normal Ca^{2+} homeostasis at *dmiro* ter-

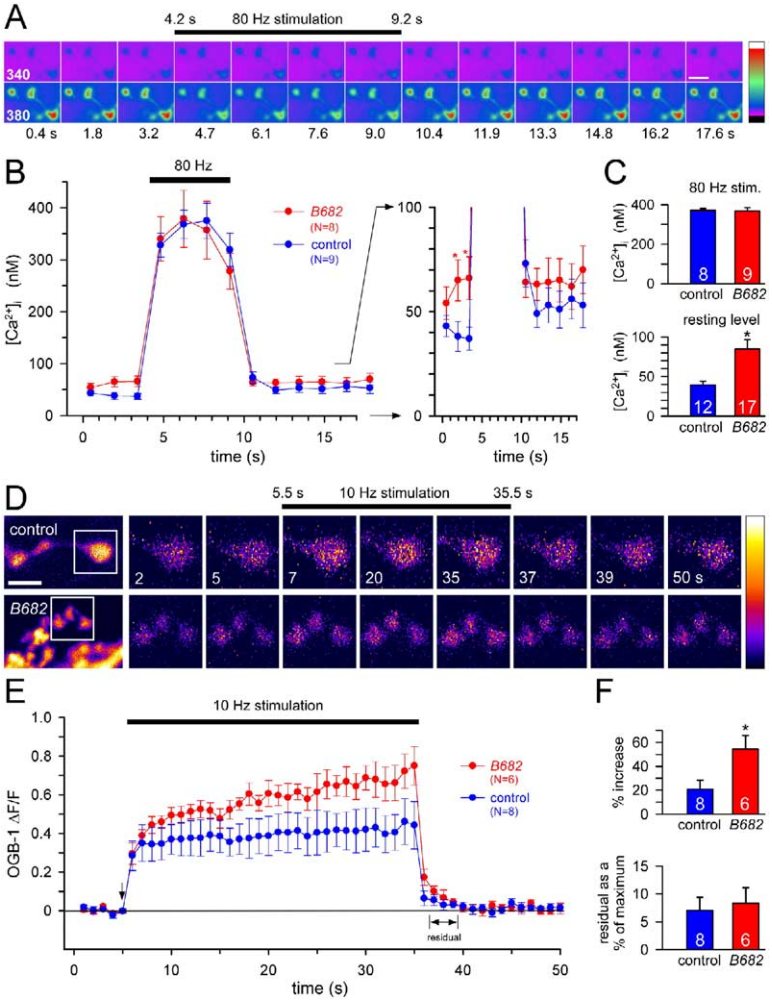

Figure 8. Presynaptic Ca^{2+} Dynamics at *dmiro* Mutant Motor Nerve Terminals Lacking Mitochondria

(A–C) Presynaptic $[Ca^{2+}]_i$ during short stimulation trains was measured using forward-filled fura-dextran and HL-6 solution containing 2 mM Ca^{2+}. (A) Images of boutons from control larva filled with fura-dextran and excited alternately with 340 nm and 380 nm light (510 nm emission). Image pairs were collected every 1.4 s. Period of nerve stimulation and fluorescence intensity scale are indicated. Scale bar, 5 μm. (B) Quantification of stimulation-evoked changes in $[Ca^{2+}]_i$ from control and *dmiro*^{B682} terminals. The difference in resting $[Ca^{2+}]_i$ is emphasized with the expanded ordinate scale to the right (asterisk, $p < 0.05$). (C) Average stimulated presynaptic peak $[Ca^{2+}]_i$ (top) and resting $[Ca^{2+}]_i$ (bottom) from control and *dmiro*^{B682} terminals (asterisk, $p < 0.05$). (D–F) Relative changes in presynaptic Ca^{2+} during long stimulation trains were measured with Oregon Green 488 BAPTA-1 (OGB-1) in HL-3 solution containing 1 mM Ca^{2+}. (D) Images of boutons from control and *dmiro*^{B682} mutant larva filled with OGB-1. Single images were collected at 1 s intervals. Period of nerve stimulation, time of image acquisition, and fluorescence intensity scale are indicated. Boxed region is 5 μm square. (E) Quantification of stimulation-evoked changes in fluorescence (*ΔF/F*) from synaptic boutons of control and *dmiro*^{B682} terminals. (F) (Top) Average % increase of fluorescence (*ΔF/F*) over the duration of the stimulus trains for control and *dmiro*^{B682} boutons (asterisk, $p < 0.05$). (Bottom) Average residual fluorescence (*ΔF/F*) measured at time points 37–39 s (indicated in [E]). All error bars represent the SEM.

minals lacking mitochondria, their significance as short-term Ca^{2+} sinks at these nerve terminals is either very limited or easily compensated by other mechanisms.

Discussion

dMiro Is Required for Anterograde Axonal Transport of Mitochondria

We have determined that the conserved GTPase dMiro is essential for the proper distribution of mitochondria into dendrites and axon terminals. Although the true cause for the slim body, the smaller muscle size, the progressive deterioration of locomotion, and the premature death of *dmiro* mutant larvae remains to be established, it is remarkable that all of these deficiencies have an exclusively neuronal origin, since they were rescued by neuronal expression of normal dMiro.

Motor nerve terminals of *dmiro* null mutants lack mitochondria, but contain relatively undisturbed numbers of synaptic vesicles. Instead of being transported, mitochondria accumulate like "strings of pearls" in neuronal somata, which indicates a traffic jam of mitochondria that are connected to MTs but cannot be transported into axons and dendrites. This defect is unlikely to be caused by a structural or functional deficit of mitochondria, since they exhibited neither an ultrastructural defect nor a reduced mitochondrial membrane potential. The altered MT organization is also unlikely to cause the defect. Since both mitochondria and vesicles employ kinesin motors for anterograde transport, one would expect that a defect of MTs affects mitochondrial and vesicular transport in qualitatively and quantitatively similar ways. However, neither the loss nor the gain of dMiro activity affected transport mechanisms of these organelles in the same way. Hence, it is unlikely that the altered organization of MTs is the primary cause of the defect in mitochondrial transport.

The mitochondrial accumulations of *dmiro* mutants are similar to the perinuclear accumulations of MT-associated mitochondria in mouse mutants of the mitochondria-associated kinesin heavy chain Kif5B (Tanaka et al., 1998). Mutations in *Drosophila* Milton, a potential adaptor protein that links mitochondria to kinesin motors, also caused mitochondrial accumulations in photoreceptor somata and a loss of mitochondria at photoreceptor terminals (Gorska-Andrzejak et al., 2003;

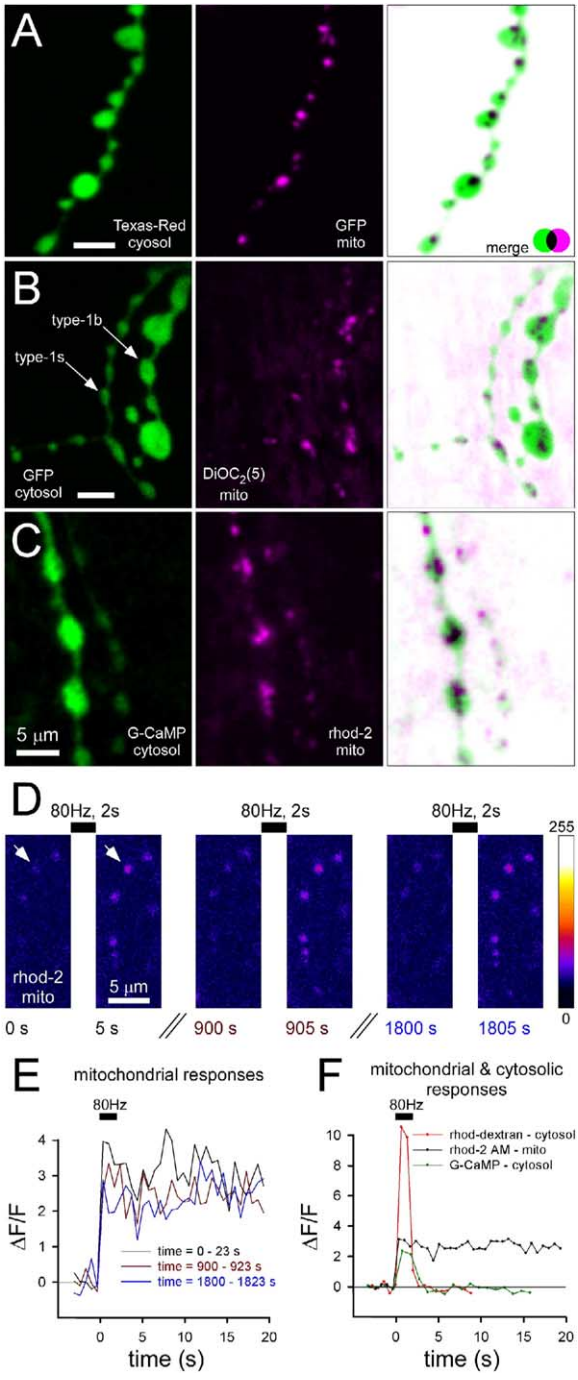

Figure 9. Ca^{2+} Uptake by Presynaptic Mitochondria at Larval NMJs during Stimulation

(A) Live MitoGFP labeling of presynaptic mitochondria (center) in type-1b boutons of wild-type (Canton S) that were forward-filled with Texas Red 10 kDa (left). Scale bar, 5 μm for all panels.

(B) Live $DiOC_2(5)$ labeling of mitochondria (center) in type-1b and 1s boutons that were labeled by presynaptic expression of cytosolic GFP (left).

(C) Live dihydrorhod-2 AM (rhod-2) labeling of mitochondria (center) in type-1b and 1s boutons expressing the cytosolic Ca^{2+} indicator G-CaMP (left). Both images were taken during stimulation at 80 Hz.

(D) Rhod-2 loaded mitochondria (as in [C]) before (0 s, first left panel) and 5 s (s) after 80 Hz stimulation (second panel from left). Stimulation was repeated at 900 s (middle) and 1800 s after the first stimulation (right). Imaging was done in HL-6 solution containing 2 mM Ca^{2+} and 7 mM L-glutamic acid. Arrows indicate a single fluorescent punctum attributed to mitochondrial Ca^{2+} uptake. Each panel represents an average of 5 images (captured 0.68 s apart).

(E) Change of rhod-2 fluorescence ($\Delta F/F$) in response to three consecutive stimulation trains was quantified for the fluorescent punctum indicated by arrows in (D).

(F) Comparison of changes in fluorescence ($\Delta F/F$) for mitochondrial rhod-2 with the cytosolic Ca^{2+} indicators rhod-dextran (0.68 s sample interval) and G-CaMP (1 s sample interval; expressed by Ok6-Gal driver) in response to 80 Hz, 2 s stimulation. Note that cytosolic Ca^{2+} rises rapidly with stimulation and then declines rapidly to baseline, while mitochondrial Ca^{2+} remains elevated after stimulation. Following stimulation, there is no elevation above baseline for the rhod-dextran $\Delta F/F$ signal, indicating that Ca^{2+} released from mitochondria occurs at such a low rate that cytosolic Ca^{2+} resting levels are unaffected.

Stowers et al., 2002). Accordingly, the mitochondrial clusters in *dmiro* mutants are consistent with an impairment of the anterograde transport machinery.

The effects of dMiro overexpression further support a role in regulating mitochondrial transport. While expression of normal dMiro protein in *dmiro* mutants restored the transport of mitochondria out of somata into axons, it also caused an abnormal accumulation of mitochondria in terminal boutons of NMJs. This new defect is apparently induced by a gain of activity since similar alterations were also observed upon overexpression of dMiro in otherwise wild-type flies. Hence, loss and gain of dMiro activity consistently alter the subcellular distribution of mitochondria in neurons in opposite ways: while loss of dMiro arrests mitochondrial transport in cell bodies, gain of dMiro activity accumulates mitochondria at terminal synaptic boutons of motor axons. Three possibilities may explain the gain-of-function phenotype: excessive anterograde movement, a failure to terminate anterograde movement, or a failure in identifying appropriate subcellular target sites. Although our study cannot distinguish among these possibilities, the opposing effects induced by loss and gain of dMiro activity consistently suggest that dMiro is required for anterograde transport of mitochondria to ensure a normal subcellular distribution. Such a role is consistent with the suggestion that small GTPases, but not heterotrimeric G proteins, regulate organelle transport along axonal MTs (Bloom et al., 1993).

Assuming that Miro proteins, like other small GTPases, provide "signaling nodes" that integrate signals to coordinate multiple downstream events (Jordan et al., 2000), Miro proteins may provide an interface between cellular signaling pathways and mitochondrial transport to control the subcellular distribution of mitochondria. Such a signal-integrating role is supported by a structural analysis of yeast Miro, showing that both GTPase domains and both Ca^{2+} binding EF-hands are required for Gem1p function (Frederick et al., 2004). Accordingly, guanine nucleotide exchange and hydrolysis factors or Ca^{2+} binding could potentially modulate dMiro activity and mitochondrial mobility at "turnaround" or stationary "target zones." However, further work will be required to resolve how mitochondrial transport might be mediated by an independent or cooperative action of Miro GTPase and EF-hand domains.

Consequences of Altering dMiro Function for the Organization of *Drosophila* NMJs

The subcellular distribution of mitochondria in neurons is assumed to be important for neuronal physiology, but direct evidence is scarce. In this study, we have uncovered a connection between presynaptic mitochondria and the structure of NMJs. The loss of dMiro activity resulted in the loss of presynaptic mitochondria, an increased number of synaptic boutons, and an altered bouton structure, suggesting that presynaptic mitochondria and/or mitochondrial proteins are important for structurally organizing NMJs. However, presynaptic mitochondria at NMJs are not required for the formation of new synaptic boutons, which contrasts with the role that has been suggested for mitochondria in dendritic spine formation (Li et al., 2004).

Li et al. (2004) manipulated the GTPases Drp1 (dynamin-related protein 1) and Opa1 (optic atrophy), which alter the morphology and distribution of mitochondria by controlling mitochondrial fission and fusion (Karbowski and Youle, 2003). Manipulations that decreased the number of mitochondria in dendrites of cultured hippocampal cells reduced the number of synapses and dendritic spines. Reciprocally, increasing dendritic mitochondrial content or activity caused an increase in the number of synapses and dendritic spines, suggesting that dendritic mitochondria are rate limiting for the support of synapses (Li et al., 2004). The contrasting lack of any correlation between synapse number and the number of presynaptic mitochondria at *dmiro* mutant NMJs may indicate different roles of pre- and postsynaptic mitochondria or differences between NMJs and central synapses. There also may be a critical difference between a complete absence and a reduction of mitochondria, since reduced numbers of mitochondria in hippocampal dendrites did not affect dendritic patterns (Li et al., 2004), while the loss of mitochondria at *dmiro* mutant NMJs caused significant presynaptic structural changes. Consistently, loss of Drp1 function in *Drosophila* neither alters the structure nor increases the number of synaptic boutons at NMJs, although the number of mitochondria is much reduced (see Verstreken et al., 2005 [this issue of *Neuron*]).

The abnormal structure of synaptic boutons at *dmiro* mutant NMJs may be linked to the abnormal organization of presynaptic MTs, as indicated by the loss of MT loops and bundles. The cause of the abnormal presynaptic MT organization at *dmiro* mutant NMJs remains unknown, but chronic ATP depletion may be excluded because missing MTs were also observed in *dmiro* mutant muscles in which the general prevalence of abnormally clustered mitochondria is unlikely to result in areas of ATP depletion.

Synaptic Transmission and Effective Ca^{2+} Clearance Persist in the Absence of Presynaptic Mitochondria

Motor nerve terminals of *dmiro* mutants, with their chronic absence of mitochondria, provide interesting insights into the role of presynaptic mitochondria in synaptic function. The high energy costs of synaptic transmission, arising mostly from the ATP dependence of synaptic vesicle exo- and endocytosis, ion pumps, transporters, and transmitter metabolism, suggest that synaptic function requires the continuous presence of mitochondria (Laughlin, 2001). Although the presynaptic defects of *dmiro* mutant nerve terminals support this notion, it is still surprising how well these synapses can adjust to the chronic lack of mitochondria. Since larval *dmiro* motor terminals can maintain basic synaptic function for at least several days, the question arises of how these terminals are supplied with ATP. Potentially, diffusion of ATP from the cell body through the motor axon, together with local glycolysis, could substitute for oxidative ATP synthesis by presynaptic mitochondria.

Motor nerve terminals that chronically lack mitochondria provide a unique opportunity for studying the role of mitochondrial Ca^{2+} uptake in transmitter release. Acute pharmacological inactivation of mitochondria at NMJs of frog, lizard, and mouse suggested that mitochondrial Ca^{2+} uptake critically limits the accumulation of presynaptic Ca^{2+} during repetitive stimulation, thereby preventing desynchronization of evoked release (David and Barrett, 2003; Talbot et al., 2003). Our recordings of presynaptic Ca^{2+} and transmitter release from *dmiro* NMJs revealed remarkable differences between nerve terminals that acutely or chronically lack mitochondrial function. Chronic absence of mitochondria caused nanomolar increases in presynaptic Ca^{2+} levels during comparable repetitive stimulation, but not micromolar increases as reported for acute manipulations (David and Barrett, 2003; Talbot et al., 2003; Suzuki et al., 2002; David, 1999; Tang and Zucker, 1997). Since mitochondrial Ca^{2+} uptake occurs at *Drosophila* motor nerve terminals, we suggest that mitochondrial Ca^{2+} uptake for Ca^{2+} homeostasis at these nerve terminals is either not required or easily compensated by other mechanisms. Assuming that the latter occurs, then it is surprising how powerful and effective these compensatory mechanisms are. A likely candidate for compensation is the endoplasmic reticulum, which interacts with mitochondria, exchanges Ca^{2+} with mitochondria, and can act as a Ca^{2+} sink (Rizzuto et al., 2000). Alternatively, Na^{+}/Ca^{2+} exchange or membrane Ca^{2+} ATPase activities may be altered.

Our study did not reveal a large, activity-dependent increase in presynaptic Ca^{2+} levels that correlated with the desynchronization of transmitter release, which contrasts with other studies in which mitochondria were acutely inactivated (David and Barrett, 2003; Talbot et al., 2003). Consequently, the desynchronization of transmitter release in *dmiro* mutants may be due either to the abnormal synaptic structure or the lack of mitochondrial ATP production impairing mobilization of synaptic vesicles in the reserve pool (Verstreken et al., 2005). In conclusion, our results reveal that the chronic loss of presynaptic mitochondria at *Drosophila* NMJs has severe consequences for presynaptic structure and neurotransmitter release, but unexpectedly mild consequences for presynaptic Ca^{2+} homeostasis.

Experimental Procedures

Experimental details regarding fly strains, the genetic screen, genetic and molecular mapping of the *dmiro* locus, subcellular fractionation, COS7 cell transfections, and the generation of *dmiro* transgenes are described in the Supplemental Data methods sections.

Mitochondria Live Imaging

Mitochondria labeled with MitoGFP were imaged in dissected third instar larvae in Schneider's or HL-6 medium, using standard confocal microscopy. To label mitochondria with MitoTracker Green FM (Molecular Probes Inc., Eugene, OR), dissected larvae were incubated in Schneider's medium containing 100 nM dye for 30 min at room temperature, washed 3× in Schneider's medium, and imaged after a 2 hr resting period. Mitochondria were stained with 3,3′-diethyloxadicarbocyanine iodide ($DiOC_2(5)$; Molecular Probes) in HL-6 solution containing 5 nM $DiOC_2(5)$ for 40 s. Cultured cells were incubated with 100 nM MitoTracker for 15 min or 6 μm JC-1 dye for 5 min, washed once, and imaged after 1 hr. Schneider medium was used for primary neuronal cell culture at 25°C and DMEM, for COS7 cells at 37°C.

Immunostainings

Dissected third instar larvae were fixed with 3.5% paraformaldehyde for 1 hr at room temperature, washed twice with PBT (PBS [pH, 7.4] containing 0.2% Triton X-100) for 10 min, blocked with PBT containing 1% BSA and 5% normal goat serum (PBTB) for 30 min, incubated with primary antibody in PBTB overnight at 4°C, washed with PBT, incubated with secondary antibody in PBTB for 1 to 2 hr at room temperature, and washed three times with PBT for 10 min. Antibodies and their dilutions were: mouse anti-CSP 1:100 (ab 49); rabbit anti-synaptotagmin 1:10,000 (DSYT-2; H. Bellen, Baylor College of Medicine, Houston, TX); goat anti-HRP Cy3-conjugated 1:300-400 (Jackson Laboratories, West Grove, PA); anti-cytochrome c oxidase 1:200 (Santa Cruz Biotechnology Inc., Santa Cruz, CA); nc82 1:10 (E. Buchner, University of Wuerzburg, Germany); anti-HRP-FITC 1:100 (Jackson Laboratories); mouse anti-milton 1:10 (T. Schwarz, Children's Hospital, Boston, MA); mouse anti-acetylated tubulin 1:1000 (Sigma, St. Louis, MO); rabbit anti-GFP Alexa488-conjugated 1:200 (Molecular Probes); rabbit or mouse anti-GFP 1:200 (Molecular Probes); goat anti-V5-FITC 1:400 (Bethyl Laboratories, Inc., Montgomery, TX); anti-rabbit FITC-conjugated mouse antibody 1:100 (Jackson Laboratories); rabbit anti-mouse Cy3-conjugated antibody 1:200 (Jackson Laboratories); anti-mouse Alexa488-conjugated 1:400 (Molecular Probes); and mouse anti-rabbit Cy3-conjugated antibody 1:200 (Jackson Laboratories).

Electron Microscopy

Dissected ventral ganglia were fixed in Trump's fixative (4% paraformaldehyde, 1% glutaraldehyde, 100 mM cacodylate buffer (CB [pH, 7.2]), 2 mM sucrose, 0.5 mM EGTA) for 1 to 2 hr at room temperature and then overnight at 4°C. After washing in CB containing 264 mM sucrose (3× for 10 min), the tissue was postfixed with 1% OsO4 in CB for 3 hr at room temperature, dehydrated in a series of ethanol dilutions (50%, 70%, 95%, and 100%) followed by propylene oxide, and embedded in Epon/Araldite. Serial cross-sections were poststained with 2% uranyl acetate and 1% lead citrate and examined by electron microscopy on a JEOL 1200 EX microscope (80 kV). Images were obtained with a Gatan Bioscan camera using digital micrograph version 3.8.1 for Gatan Microscopy Suite.

For NMJs, the procedures were similar, but the fixative contained 1% paraformaldehyde and 3% glutaraldehyde and lacked sucrose; 2% OsO_4 (1 hr) was used in postfixation. Staining was in 4% uranyl acetate and Reynolds' lead citrate. Images were obtained on a Hitachi H7000 electron microscope using an AMT XR-60 camera and AMT software version 5.0. Reconstructions were made using IMOD version 3.1.0.

Electrophysiology

Intracellular whole-cell recordings were made with a single microelectrode filled with 3 M KCl (20–40 MΩ) essentially as described (Dawson-Scully et al., 2000). All recordings were made from muscle 6, segment A4 or A5 of 3rd instar larvae in HL-3 medium containing 1 mM Ca^{2+}, except where specified. For electrotonic stimulation, 5 μM TTX was slowly perfused until AP-elicited EJPs were fully blocked. Subsequently, electrotonic EJPs were elicited by increasing the stimulus intensity 10-fold.

Calcium Imaging

Motor neuron terminals were loaded with fura-dextran (10 kDa), Oregon Green 488 BAPTA-1 (10 kDa), or rhod-dextran (10 kDa; all from Molecular Probes) as described (Macleod et al., 2004, 2002). Mitochondria were loaded with dihydrorhod-2 AM (Molecular Probes) by incubating dissected larvae for 90 min at 4°C in Schneider's medium containing 6 μM dye, 0.3% DMSO, and 0.06% pluronic acid and were rinsed in dye-free Schneider's medium for 90 min at room temperature. Calcium imaging with cytosolic Ca^{2+} indicators and its analysis using ImageJ software (http://rsb.info.nih.gov/ij/) was performed as described (Macleod et al., 2004).

Statistical Analysis

Comparisons between mutants and controls (*FRT82B*) were made using Student's t test or one-way ANOVA. Unless otherwise indicated, $p < 0.05$ was deemed significant.

Supplemental Data

Supplemental data include five figures, one table, Supplemental Experimental Procedures, and Supplemental References and can be found with this article online at http://www.neuron.org/cgi/content/full/cgi/47/3/379/DC1.

Acknowledgments

This study is dedicated to Konrad Zinsmaier, Sr. (1921-2004) for his invaluable support to K.E.Z. We thank Patty Jansma, Jinhui Zhang, and the University of Arizona DNA sequencing facility for their help. We thank Patrik Verstreken, Hugo Bellen, and Tom Schwarz, for critical comments and sharing unpublished information. We thank Bill Saxton, Tom Schwarz, Hugo Bellen, Mani Ramaswami, Erich Buchner, and Alan Nighorn for fly strains or antibodies. We thank Joanne Pearce for early contributions and Gurbir Sekhon for help with the 3-D reconstruction. G.S. was supported by a Summer Research Studentship from the Natural Sciences and Engineering Research Council of Canada. M.S. was supported by an REU Award (NSF) through the Undergraduate Biology Research Program of the University of Arizona. This study was supported by grants to K.E.Z. (National Science Foundation) and to H.L.A. (Natural Sciences and Engineering Research Council of Canada).

Received: November 18, 2004
Revised: April 21, 2005
Accepted: June 21, 2005
Published: August 3, 2005

References

Babcock, M.C., Stowers, R.S., Leither, J., Goodman, C.S., and Pallanck, L.J. (2003). A genetic screen for synaptic transmission mutants mapping to the right arm of chromosome 3 in Drosophila. Genetics *165*, 171–183.

Benzer, S. (1967). Behavioral mutants of Drosophila isolated by countercurrent distribution. Proc. Natl. Acad. Sci. USA *58*, 1112–1119.

Bindokas, V.P., Lee, C.C., Colmers, W.F., and Miller, R.J. (1998). Changes in mitochondrial function resulting from synaptic activity in the rat hippocampal slice. J. Neurosci. *18*, 4570–4587.

Bloom, G.S., Richards, B.W., Leopold, P.L., Ritchey, D.M., and Brady, S.T. (1993). GTPγS inhibits organelle transport along axonal microtubules. J. Cell Biol. *120*, 467–476.

Bowman, A.B., Kamal, A., Ritchings, B.W., Philp, A.V., McGrail, M., Gindhart, J.G., and Goldstein, L.S. (2000). Kinesin-dependent axonal transport is mediated by the sunday driver (SYD) protein. Cell *103*, 583–594.

Chada, S.R., and Hollenbeck, P.J. (2004). Nerve growth factor signaling regulates motility and docking of axonal mitochondria. Curr. Biol. *14*, 1272–1276.

Chen, B., Chu, T., Harms, E., Gergen, J.P., and Strickland, S. (1998). Mapping of Drosophila mutations using site-specific male recombination. Genetics *149*, 157–163.

Chen, H., Detmer, S.A., Ewald, A.J., Griffin, E.E., Fraser, S.E., and Chan, D.C. (2003). Mitofusins MFN1 and MFN2 coordinately regulate mitochondrial fusion and are essential for embryonic development. J. Cell Biol. *160*, 189–200.

Crosby, A.H., and Proukakis, C. (2002). Is the transportation highway the right road for hereditary spastic paraplegia? Am. J. Hum. Genet. *71*, 1009–1016.

David, G. (1999). Mitochondrial clearance of cytosolic Ca^{2+} in stimulated lizard motor nerve terminals proceeds without progressive elevation of mitochondrial matrix. J. Neurosci. *19*, 7495–7506.

David, G., and Barrett, E.F. (2000). Stimulation-evoked increases in cytosolic [Ca(2+)] in mouse motor nerve terminals are limited by mitochondrial uptake and are temperature-dependent. J. Neurosci. *20*, 7290–7296.

David, G., and Barrett, E.F. (2003). Mitochondrial Ca^{2+} uptake prevents desynchronization of quantal release and minimizes depletion during repetitive stimulation of mouse motor nerve terminals. J. Physiol. *548*, 425–438.

David, G., Barrett, J.N., and Barrett, E.F. (1998). Evidence that mitochondria buffer physiological Ca^{2+} loads in lizard motor nerve terminals. J. Physiol. *509*, 59–65.

Dawson-Scully, K., Bronk, P., Atwood, H.L., and Zinsmaier, K.E. (2000). Cysteine-string protein increases the calcium sensitivity of neurotransmitter exocytosis in Drosophila. J. Neurosci. *20*, 6039–6047.

De Vos, K.J., Sable, J., Miller, K.E., and Sheetz, M.P. (2003). Expression of phosphatidylinositol (4,5) bisphosphate-specific pleckstrin homology domains alters direction but not the level of axonal transport of mitochondria. Mol. Biol. Cell *14*, 3636–3649.

Fransson, A., Ruusala, A., and Aspenstrom, P. (2003). Atypical Rho GTPases have roles in mitochondrial homeostasis and apoptosis. J. Biol. Chem. *278*, 6495–6502.

Frederick, R.L., McCaffery, J.M., Cunningham, K.W., Okamoto, K., and Shaw, J.M. (2004). Yeast Miro GTPase, Gem1p, regulates mitochondrial morphology via a novel pathway. J. Cell Biol. *167*, 87–98.

Goldstein, L.S. (2001). Kinesin molecular motors: transport pathways, receptors, and human disease. Proc. Natl. Acad. Sci. USA *98*, 6999–7003.

Goldstein, L.S. (2003). Do disorders of movement cause movement disorders and dementia? Neuron *40*, 415–425.

Gorska-Andrzejak, J., Stowers, R.S., Borycz, J., Kostyleva, R., Schwarz, T.L., and Meinertzhagen, I.A. (2003). Mitochondria are redistributed in Drosophila photoreceptors lacking milton, a kinesin-associated protein. J. Comp. Neurol. *463*, 372–388.

Gunawardena, S., and Goldstein, L.S. (2001). Disruption of axonal transport and neuronal viability by amyloid precursor protein mutations in Drosophila. Neuron *32*, 389–401.

Hollenbeck, P.J. (1996). The pattern and mechanisms of mitochondrial transport in axons. Front. Biosci. *1*, d91–d102.

Hurd, D.D., and Saxton, W.M. (1996). Kinesin mutations cause motor neuron disease phenotypes by disrupting fast axonal transport in Drosophila. Genetics *144*, 1075–1085.

Jordan, J.D., Landau, E.M., and Ivenger, R. (2000). Signaling networks: the origins of cellular multitasking. Cell *103*, 193–200.

Kammermeier, L., Spring, J., Stierwald, M., Burgunder, J.M., and Reichert, H. (2003). Identification of the Drosophila melanogaster homolog of the human spastin gene. Dev. Genes Evol. *213*, 412–415.

Karbowski, M., and Youle, R.J. (2003). Dynamics of mitochondrial morphology in healthy cells and during apoptosis. Cell Death Differ. *10*, 870–880.

Laughlin, S.B. (2001). Energy as a constraint on the coding and processing of sensory information. Curr. Opin. Neurobiol. *11*, 475–480.

Li, Z., Okamoto, K., Hayashi, Y., and Sheng, M. (2004). The importance of dentritic mitochondria in the morphogenesis and plasticity of spines and synapses. Cell *119*, 873–887.

Macleod, G.T., Hegstrom-Wojtowicz, M., Charlton, M.P., and Atwood, H.L. (2002). Fast calcium signals in Drosophila motor neuron terminals. J. Neurophysiol. *88*, 2659–2663.

Macleod, G.T., Marin, L., Charlton, M.P., and Atwood, H.L. (2004). Synaptic vesicles: test for a role in presynaptic calcium regulation. J. Neurosci. *24*, 2496–2505.

Miller, K.G., and Sheetz, M.P. (2004). Axonal mitochondrial transport and potential are correlated. J. Cell Sci. *117*, 2791–2804.

Morris, R.L., and Hollenbeck, P.J. (1993). The regulation of bidirectional mitochondrial transport is coordinated with axonal outgrowth. J. Cell Sci. *104*, 917–927.

Nguyen, P.V., Marin, L., and Atwood, H.L. (1997). Synaptic physiology and mitochondrial function in crayfish tonic and phasic motor neurons. J. Neurophysiol. *78*, 281–294.

Ohnuma, K., Kazawa, T., Ogawa, S., Suzuki, N., Miwa, A., and Kijima, H. (1999). Cooperative Ca^{2+} removal from presynaptic terminals of the spiny lobster neuromuscular junction. Biophys. J. *76*, 1819–1834.

Rintoul, G.L., Filiano, A.J., Brocard, J.B., Kress, G.J., and Reynolds, I.J. (2003). Glutamate decreases mitochondrial size and movement in primary forebrain neurons. J. Neurosci. *23*, 7881–7888.

Rizzuto, R., Bernardi, P., and Pozzan, T. (2000). Mitochondria as all-round players of the calcium game. J. Physiol. *529*, 37–47.

Shepherd, G.M., and Harris, K.M. (1998). Three-dimensional structure and composition of CA3→CA1 axons in rat hippocampal slices: implications for presynaptic connectivity and compartmentalization. J. Neurosci. *18*, 8300–8310.

Sherwood, N.T., Sun, Q., Xue, M., Zhang, B., and Zinn, K. (2004). Drosophila spastin regulates synaptic microtubules networks and is required for normal motor function. PLoS Biol. *2(12)*, e429. 10.1371/journal.pbio.0020429

Stowers, R.S., and Schwarz, T.L. (1999). A genetic method for generating Drosophila eyes composed exclusively of mitotic clones of a single genotype. Genetics *152*, 1631–1639.

Stowers, R.S., Megeath, L.J., Gorska-Andrzejak, J., Meinertzhagen, I.A., and Schwarz, T.L. (2002). Axonal transport of mitochondria to synapses depends on Milton, a novel Drosophila protein. Neuron *36*, 1063–1077.

Suzuki, S., Osani, M., Mitsumoto, N., Akita, T., Narita, K., Kijima, H., and Kuba, K. (2002). Ca^{2+}-dependent Ca^{2+} clearance via mitochondrial uptake and plasmalemmal extrusion in frog motor nerve terminals. J. Neurophysiol. *87*, 1816–1823.

Talbot, J.D., David, G., and Barrett, E.F. (2003). Inhibition of mitochondrial Ca^{2+} uptake affects phasic release from motor nerve terminals differently depending on external [Ca2+]. J. Neurophysiol. *90*, 491–502.

Tanaka, Y., Kanai, Y., Okada, Y., Nonaka, S., Takeda, S., Harada, A., and Hirokawa, N. (1998). Targeted disruption of mouse conventional kinesin heavy chain, Kif5B, results in abnormal perinuclear clustering of mitochondria. Cell *93*, 1147–1158.

Tang, Y., and Zucker, R.S. (1997). Mitochondrial involvement in post-tetanic potentiation of synaptic transmission. Neuron *18*, 483–491.

Trollinger, D.R., Cascio, W.E., and Lemasters, J.J. (1997). Selective loading of Rhod 2 into mitochondria shows mitochondrial Ca^{2+} transients during the contractile cycle in adult rabbit cardiac myocytes. Biochem. Biophys. Res. Commun. *236*, 738–742.

Trotta, N., Orso, G., Rossetto, M.G., Daga, A., and Broadie, K. (2004). The hereditary spastic paraplegia gene, spastin, regulates microtubule stability to modulate synaptic structure and function. Curr. Biol. *14*, 1135–1147.

Vale, R.D. (2003). The molecular toolbox for intracellular transport. Cell *112*, 467–480.

Verstreken, P., Ly, C.V., Venken, K.J.T., Koh, T.W., Zhou, Y., and Bellen, H.J. (2005). Synaptic mitochondria are critical for mobilization of reserve pool vesicles at Drosophila neuromuscular junctions. Neuron *47*, this issue, 365–378.

Welte, M.A. (2004). Bidirectional transport along microtubules. Curr. Biol. *14*, R525–R537.

Wong-Riley, M., and Carroll, E.W. (1984). Effect of impulse blockage on cytochrome oxidase activity in monkey visual system. Nature *307*, 262–264.

Wong-Riley, M.T., and Welt, C. (1980). Histochemical changes in cytochrome oxidase of cortical barrels after vibrissal removal in neonatal and adult mice. Proc. Natl. Acad. Sci. USA *77*, 2333–2337.

Wucherpfennig, T., Wilsch-Brauninger, M., and Gonzalez-Gaitan, M. (2003). Role of Drosophila Rab5 during endosomal trafficking at the synapse and evoked neurotransmitter release. J. Cell Biol. *161*, 609–624.